

# MATHEMATICAL FOUNDATION FOR THE GENERALISED BRILLOUIN ZONE OF M-BANDED TOEPLITZ OPERATORS.

YANNICK DE BRUIJN  AND ERIK ORVEHED HILTUNEN 

**ABSTRACT.** We show that the spectrum of the open-boundary limit of banded Toeplitz matrices is real whenever the associated symbol function is real-valued along a closed polar curve. Building on this result, we develop both analytical and numerical methods to symmetrise a class of banded non-Hermitian Toeplitz matrices whose asymptotic spectra are real. Finally, we provide a rigorous mathematical foundation for the generalised Brillouin zone, a concept widely used in non-Hermitian physics, by proving that it coincides with the polar curve on which the symbol function takes real values.

**Mathematics Subject Classification (MSC2020):** 15A18 15B05, 65F15

**Keywords:** Non-Hermitian Hamiltonian, generalised Brillouin zone, density of states, asymptotic spectra, non-Bloch Band theory, open boundary conditions.

## 1. INTRODUCTION

Toeplitz matrices are a class of structured matrices in which each diagonal is filled with the same value. These matrices frequently appear as Hamiltonians that model systems with a periodic structure, for instance, periodic media or metamaterials. The so called *open limit* of the spectrum of Toeplitz matrices, see [9] for an overview, is of particular interest as it corresponds to the asymptotic spectrum of a finite Toeplitz matrix which is growing in dimension. For non-Hermitian matrices, it is widely understood that the open spectrum cannot be described using conventional Floquet-Bloch band theory. In the specific case of tridiagonal Toeplitz matrices, it was demonstrated in [4, 12] that the open limit is instead accurately captured by complex Floquet-Bloch boundary conditions, where the imaginary part of the quasimomentum is constant and non-zero. In the more general  $m$ -banded case, the imaginary part of the Bloch quasimomentum may vary across the spectrum and is specified by the generalised Brillouin zone [4, 6, 27, 39, 41]. Although the generalised Brillouin zone is a widely used tool in the physics literature, a number of mathematical questions remain unanswered.

An open problem to this date is to find a criterion on the symbol function that guarantees the open limit to be real-valued. This result has been conjectured in [31], and we will present a proof under stronger assumptions. We will prove that if it is possible to find a closed polar curve along which the symbol function evaluates to real numbers, the open limit will be real. The Toeplitz matrix corresponding to the symbol function evaluated along this polar curve will be Hermitian. In particular, we will demonstrate that both the open limit and the density of states remain unchanged under this transformation. Furthermore, we illustrate numerically that the eigenvalues converge pointwise, which demonstrates that the symbol transform can be seen as an asymptotic similarity transform between a class of non-Hermitian and Hermitian Toeplitz matrices.

We revisit some concepts from Toeplitz theory that were known since the 1960s [24, 33, 35], in particular, the results from [30, 35, 36] will allow us to define the right polar curve on which we evaluate the symbol function. We illustrate that the polar curve is the natural generalisation of complex band structure in tridiagonal Toeplitz matrices [3, 10, 11]. Moreover, we will make an important connection between this polar curve and generalised Brillouin zone, and demonstrate that our method has a widespread use in the asymptotic study of non-Hermitian Bloch Hamiltonians explored in condensed matter physics.

An important application of our method is in the realm of non-Hermitian physics. A prominent example is the non-Hermitian skin effect, which refers to the localisation the bulk eigenmodes at the boundary of a non-Hermitian open system [6, 14, 27, 39, 41]. This new framework enables to extend the tight binding Hamiltonians with non-reciprocal coupling, as introduced by Hatano and Nelson [19, 20] to models with long range coupling.

This paper is organised as follows. In Section 2, we recall the most important results from Toeplitz theory and present a criterion on the symbol function that guarantees the reality of the open limit. We demonstrate that the open limit remains unchanged under a deformation of the torus on which the symbol function is evaluated. Moreover, we provide numerical evidence that, in the limit of large matrix size, the two sets of eigenvalues of the finite Toeplitz matrices converge. We prove that under the assumptions that the open limit is real, the density of states of a non-Hermitian matrix Toeplitz matrices agrees with that of the Hermitian matrix which is generated by deforming the unit torus to the generalised Brillouin zone. In Section 3 we link the results from Section 2 and provide a mathematical foundation for the generalised Brillouin zone. In Section 4 we conclude on our work and present future works and possible applications of the newly developed theory. The Matlab code that supports the findings of this article is openly available in Section 5.

## 2. TOEPLITZ ANALYSIS

This paper is devoted to the study of the asymptotic spectra of banded Toeplitz matrices. A Toeplitz operator  $\mathbf{A}$  is generated by the sequence  $\{a_n\}_{n=-\infty}^{\infty}$  and is given by the semi-infinite matrix,

$$\mathbf{A} = \begin{pmatrix} a_0 & a_{-1} & a_{-2} & a_{-3} & \cdots \\ a_1 & a_0 & a_{-1} & a_{-2} & \cdots \\ a_2 & a_1 & a_0 & a_{-1} & \cdots \\ a_3 & a_2 & a_1 & a_0 & \cdots \\ \vdots & \vdots & \vdots & \vdots & \ddots \end{pmatrix}. \quad (2.1)$$

We define a  $m$ -banded Toeplitz operator as

$$\mathbf{A}_m = \begin{cases} \mathbf{A}_{i,j}, & \text{for } |i - j| < m, \\ 0, & \text{for } |i - j| \geq m. \end{cases} \quad (2.2)$$

We will illustrate our results on Toeplitz matrices with non-reciprocal algebraic off-diagonal decay, that is

$$\begin{cases} a_k = \mathcal{O}(|k|^{-\kappa}), & k > 0, \\ a_k = \mathcal{O}(|k|^{-\rho}), & k < 0. \end{cases} \quad (2.3)$$

A Toeplitz operator is a bounded operator on  $\ell^2$  if and only if it is generated by a function  $f \in L^\infty$  [33]. This generating function is commonly referred to as the *symbol function* as its Fourier coefficients generate the sequence  $\{a_k\}_{n=-\infty}^{\infty}$ , that is

$$f(z) = \sum_{k=-\infty}^{\infty} a_k z^{-k}. \quad (2.4)$$

For a  $m$ -banded Toeplitz operator (2.2), the symbol function is given by the finite Laurent polynomial,

$$f_m(z) = \sum_{k=-m}^m a_k z^{-k}. \quad (2.5)$$

In the sequel of this paper, we shall refer to the Toeplitz operator  $\mathbf{A}$ , specified in equation (2.1), by the notation  $\mathbf{A} = \mathbf{T}(f)$  and for the banded Toeplitz operator (2.2), by  $\mathbf{A}_m = \mathbf{T}(f_m)$ . We note that the symbol function  $f_m$  is a special case of  $f$ , obtained by setting  $a_j = 0$  for all  $|j| > m$ .

We now define the region of non-trivial winding. We let  $\mathbb{T}$  denote the one dimensional unit circle in  $\mathbb{C}$ , that is  $\mathbb{T} = e^{-i[0, 2\pi]}$ , then

$$\sigma_{\text{wind}} := \{\lambda \in \mathbb{C} \setminus f(\mathbb{T}) : \text{wind}(f(\mathbb{T}), \lambda) \neq 0\}. \quad (2.6)$$

The spectrum of a Toeplitz operator is given by the following result [1, Theorem 1.17].

**Theorem 2.1** (Gohberg). *The operator  $\mathbf{T}(f)$  is Fredholm on  $\ell^2$  if and only if  $f(e^{i\alpha}) \neq 0$ ,  $\forall \alpha \in [0, 2\pi)$ , in which case*

$$\text{Ind } \mathbf{T}(f) = -\text{wind}(f(\mathbb{T}), 0) \quad (2.7)$$

and the spectrum is given by

$$\sigma(\mathbf{T}(f)) = f(\mathbb{T}) \cup \sigma_{\text{wind}}, \quad (2.8)$$

where  $\sigma_{\text{wind}}$  was defined in (2.6).

For later application, we will introduce the spectra of large truncated Toeplitz operators. To define a finite Toeplitz matrix, we introduce the projection operator,

$$\mathbf{P}_n : \ell^2(\mathbb{N}, \mathbb{C}) \rightarrow \ell^2(\mathbb{N}, \mathbb{C}) \quad (2.9)$$

$$(x_1, x_2, x_3, \dots) \mapsto (x_1, \dots, x_n, 0, 0, \dots). \quad (2.10)$$

A finite Toeplitz matrix is derived from a Toeplitz operator by performing the following truncation,

$$\mathbf{T}_n(f) := \mathbf{P}_n \mathbf{T}(f) \mathbf{P}_n. \quad (2.11)$$

We will be particularly interested in finding the smallest set on which the eigenvalues will cluster as the matrix dimension becomes large. The limiting spectrum of a finite but growing Toeplitz matrix will be referred to as the *open limit* and is defined as

$$\sigma_{\text{open}}(\mathbf{T}(f)) := \lim_{n \rightarrow \infty} \sigma(\mathbf{T}_n(f)). \quad (2.12)$$

A useful characterisation of the limiting set has been presented in [1, Section 5.8], with the foundational paper being [30].

**Theorem 2.2** (Schmidt-Spitzer). *Let  $f_m$  be a Laurent polynomial as defined in (2.5), then*

$$\lim_{n \rightarrow \infty} \sigma(\mathbf{T}_n(f)) = \bigcap_{r \in (0, \infty)} \sigma\left(\mathbf{T}(f(r\mathbb{T}))\right) \quad (2.13)$$

$$= \{\lambda \in \mathbb{C} : |z_m(\lambda)| = |z_{m+1}(\lambda)|\}, \quad (2.14)$$

where  $z_i(\lambda)$  are the roots of the polynomial equation  $z^m(f_m(z) - \lambda)$  sorted in ascending magnitude, that is,  $0 < |z_1(\lambda)| \leq |z_2(\lambda)| \leq \dots \leq |z_{2m}(\lambda)|$ .

Tracking the magnitude of the middle root also plays a central role in pseudoeigenvectors construction as roots with  $|z_{m+1}(\lambda)| < 1$  generate exponentially localised pseudoeigenvectors. An explicit construction is given in [10] and a visualisation can be found in Figure 3.1. The representation of the open limit given by (2.14) allows to deduce topological and analytical properties [13]. First, the set equals the union of a finite number of pairwise disjoint open analytic arcs and a finite number of the so-called *degenerate points*. We say that  $\lambda \in \{\lambda \in \mathbb{C} : |z_m(\lambda)| = |z_{m+1}(\lambda)|\}$  is a degenerate point if the polynomial  $f_m(z) - \lambda$  has confluent roots. It is not hard to see that this is the case for at most  $2m - 1$  discrete roots which are characterised by the roots of  $f'_m(z) = 0$  and therefore represent a set of measure 0 in the complex plane. The connectedness of the spectrum of Toeplitz operators was first established by Widom in [36]. A similar result for the open limit was first demonstrated in [35].

**Theorem 2.3** (Ullman). *Let  $f_m$  be a Laurent polynomial, then  $\sigma_{\text{open}}(\mathbf{T}(f_m))$  is a connected set.*

**2.1. Criteria for real asymptotic spectra of non-Hermitian Toeplitz matrices.** An important class of non-Hermitian Toeplitz matrices includes those with real spectra, often termed pseudo-Hermitian Toeplitz matrices. In this section, our focus will be on examining conditions under which the open limit, that is, finite matrices approaching infinite size, exhibit real spectra.

**Definition 2.4.** The symbol function  $f_m$  is *collapsed* at  $p \in \mathbb{C}$  if  $p = f_m(re^{i\alpha_1}) = f_m(re^{i\alpha_2})$ ,  $\alpha_1 \neq \alpha_2$ .

Consider the following polynomial

$$z^m(f_m(z) - \lambda) = \prod_{i=1}^{2m} (z - z_i(\lambda)) \quad (2.15)$$

and suppose the roots are sorted in ascending magnitude,

$$|z_1(\lambda)| \leq \dots \leq |z_m(\lambda)| \leq |z_{m+1}(\lambda)| \leq \dots \leq |z_{2m}(\lambda)|. \quad (2.16)$$

Let us define the following set,

$$\mathbf{Z}(f_m) := \{z_m, z_{m+1} \in \mathbb{C} : |z_m(\lambda)| = |z_{m+1}(\lambda)|, \text{ for some } \lambda \in \mathbb{R}\}. \quad (2.17)$$

It is easy to see that  $\mathbf{Z}(f_m) \subseteq f_m^{-1}(\mathbb{R})$ , where  $f_m^{-1}(\mathbb{R})$  denotes the set of preimages or roots of  $f_m(z) - \lambda = 0$  for  $\lambda \in \mathbb{R}$ . Moreover, it follows from the definition of the set in (2.17) that,

$$\{\lambda \in \mathbb{R} : |z_m(\lambda)| = |z_{m+1}(\lambda)|\} = \{f_m(z) : z \in \mathbf{Z}(f_m)\}. \quad (2.18)$$

A priori, it is possible for some of the roots in (2.15) to become confluent. Such roots are characterised by the fact that they are also roots of  $f'_m(z)$ . Since  $f'_m$  has at most  $2m - 1$  roots, there are at most  $2m - 1$  confluent roots independent of  $\lambda$ . We present the following technical assumption.

**Assumption 2.5.** For  $z \in \mathbf{Z}(f_m) \setminus \mathbb{R}$  then  $f'_m(z) \neq 0$ , and for  $z \in \mathbf{Z}(f_m) \cap \mathbb{R}$  then  $f''_m(z) \neq 0$ .

Moreover, the set  $\mathbf{Z}(f_m)$  together with Assumption 2.5 avoids confluent roots and, at first glance, might seem difficult to visualise, but has an intuitive visual representation when plotting the complex band structure. Namely, if the main complex band does not touch or intersect other complex bands, see Figure 2.1 (A), then must hold that  $|z_{m-1}| < |z_m| = |z_{m+1}| < |z_{m+2}|$ . We have another important observation on the structure of the set  $\mathbf{Z}(f_m)$  under Assumption 2.5.

**Remark 2.6.** Suppose that Assumption 2.5 is satisfied, then the set  $\mathbf{Z}(f_m)$  cannot contain complex confluent roots, because the roots of  $f_m(z) - \lambda$  appear in complex-conjugate pairs. However, the set  $\mathbf{Z}(f_m)$  may contain real-valued confluent roots, as long as  $f''_m(z) \neq 0$  for  $z \in \mathbb{R}$ .

In the sequel, we will introduce some more structure on the geometry of the set  $\mathbf{Z}(f_m)$ .

**Definition 2.7.** We define a *polar curve* as the set parametrised by polar coordinates such that

$$p(e^{i\theta}) = r(\theta)e^{i\theta}, \quad \theta \in [-\pi, \pi], \quad (2.19)$$

for some function  $r : [-\pi, \pi] \rightarrow (0, \infty)$  describing the radius as function of the angle  $\theta$ . For ease of notation, we will often denote the polar curve as  $p(\mathbb{T})$ , where  $\mathbb{T}$  is the one-dimensional torus.

The next result relates the geometry of the set  $\mathbf{Z}(f_m)$  to the analytical properties of the complex band structure.

**Lemma 2.8.** *If the set  $\mathbf{Z}(f_m)$  is spanned by a polar curve and Assumption 2.5 holds, then  $\lambda(\alpha)$  is strictly monotone in  $\alpha$  on the sets  $(-\pi, 0)$  and  $(0, \pi)$ .*

*Proof.* We start by noting that  $\lambda(\alpha) = f_m(e^{i(\alpha+i\beta(\alpha))})$ . Therefore, it follows that

$$\frac{d}{d\alpha} \lambda(\alpha) = \frac{d}{d\alpha} f_m(e^{i(\alpha+i\beta(\alpha))}) = f'_m(e^{i(\alpha+i\beta)}) \left( e^{i(\alpha+i\beta)} i \underbrace{\left( 1 + i \frac{d\beta}{d\lambda} \frac{d\lambda}{d\alpha} \right)}_{\neq 0} \right). \quad (2.20)$$

By Assumption 2.5 for any element  $z \in \mathbf{Z}(f)$  it follows  $f'_m(z) = 0$  if  $z \in \mathbb{R}$ , correspondingly  $\alpha \in \{0, \pm\pi\}$ . As a consequence,  $\lambda(\alpha)$  is strictly monotone in the intervals  $(-\pi, 0)$  and  $(0, \pi)$ .  $\square$

By the implicit function theorem, restricting to either  $(-\pi, 0)$  or  $(0, \pi)$ , the function  $\alpha(\lambda)$  is strictly monotone. As a consequence of Lemma 2.8, in the case where  $\mathbf{Z}(f_m)$  is spanned by a polar curve the set  $\mathbf{Z}(f_m)$  admits a parametrisation by the complex band structure, that is,  $p(e^{i\alpha}) = e^{i(\alpha+i\beta(\alpha))}$  and it follows that,

$$\mathbf{Z}(f_m) = \bigcup_{\alpha \in [-\pi, \pi]} p(e^{i\alpha}). \quad (2.21)$$

The motivation behind this polar curve  $p(\mathbb{T})$  is the following. For tridiagonal Toeplitz operators, as demonstrated in [3, 11], a unique  $\tilde{r}$  exists such that  $\bigcap_{r>0} \sigma(\mathbf{T}(f(r\mathbb{T}))) = \sigma(\mathbf{T}(f(\tilde{r}\mathbb{T})))$ . This arises because in the bulk, the complex Floquet parameter is fixed to the rate of non-reciprocity  $\tilde{r} = e^{-\beta}$  for constant  $\beta$ . However, for general  $m$ -banded Toeplitz operators, this condition does not hold, that is, there is no single  $r$  for which the symbol function  $f(r\mathbb{T})$  will be collapsed onto  $\sigma_{\text{open}}$ . Subsequently, it is not enough to evaluate the symbol function on the scaled torus and we will allow more general homotopic deformations of the unit circle. Along the polar curve  $p(\mathbb{T})$ , we have the following result.

**Lemma 2.9.** *For any  $z \in p(\mathbb{T})$ , such that  $z \in \mathbb{C} \setminus \mathbb{R}$ , the symbol  $f_m(z)$  is collapsed.*

*Proof.* Since the complex band structure is defined for  $\lambda \in \mathbb{R}$  and since the coefficients of the Laurent polynomial  $f_m$  are real, for any root  $z$  of  $f_m(z) - \lambda = 0$  it also holds that  $f_m(\bar{z}) - \lambda = 0$ . Since by assumption  $z \in \mathbb{C} \setminus \mathbb{R}$  it must hold that  $\arg(z) \neq \arg(\bar{z})$ , which completes the proof.  $\square$

The following result is one of our principal theorems, providing a sufficient condition that guarantees the reality of the spectrum of the open limit.

**Theorem 2.10.** Suppose that  $\mathbf{Z}(f_m)$  is spanned by a polar curve  $p(\mathbb{T})$  defined in (2.21) and suppose that Assumption 2.5 is met, then it holds that

$$\lim_{n \rightarrow \infty} \sigma(\mathbf{T}_n(f_m)) = \bigcup_{\alpha \in [-\pi, \pi]} f_m(e^{i(\alpha+i\beta(\alpha))}) \subset \mathbb{R}. \quad (2.22)$$

*Proof.* We start by demonstrating that  $\sigma_{\text{open}}(\mathbf{T}(f)) \subseteq \mathbb{R}$ . Suppose for contradiction that there exists a  $p \in \sigma_{\text{open}}(\mathbf{T}(f))$ , such that  $p \in \mathbb{C} \setminus \mathbb{R}$ . Consider the interval  $[\lambda_1, \lambda_2] := \sigma_{\text{open}} \cap \mathbb{R} \neq \emptyset$ , and take any  $q \in (\lambda_1, \lambda_2)$ . By Theorem 2.3 we know that  $\sigma_{\text{open}}(\mathbf{T}(f))$  is a connected set, so there exists a continuous path  $\tau : [0, 1] \rightarrow \mathbb{C}$  such that  $\tau(0) = q$  and  $\tau(1) = p$ . We can choose the path such that  $\tau(t) \in \sigma_{\text{open}}(\mathbf{T}(f))$ ,  $\forall t \in [0, 1]$ . Note that there is a value  $r_0 > 0$  so that  $f(r_0 \mathbb{T})$  is collapsed at  $\tau(0)$  on the real axis.

By assumption  $\alpha(\lambda)$  is continuous, as otherwise  $\mathbf{Z}(f_m)$  is not spanned by a polar curve. Without loss of generality, let us restrict ourselves to the case where  $\alpha(\lambda) \in [0, \pi]$ . In the limit for  $\varepsilon > 0$ , then  $\tau(\varepsilon) \in \mathbb{C} \setminus \mathbb{R}$ , by Theorem 2.2 there exist roots  $|z_m(\tau(\varepsilon))| = |z_{m+1}(\tau(\varepsilon))|$ , such that

$$f_m(z_m(\tau(\varepsilon))) = f_m(z_{m+1}(\tau(\varepsilon))) = \tau(\varepsilon). \quad (2.23)$$

We know by Lemma 2.8 that for  $\lambda \in [\lambda_1, \lambda_2]$  the band function  $\alpha(\lambda)$  is monotone at  $[0, \pi]$ , therefore  $\alpha(\lambda) = 0$  and  $\alpha(\lambda) = \pi$  can occur only at the endpoints  $\lambda_1$  or  $\lambda_2$ . For  $q \in (\lambda_1, \lambda_2)$  satisfying  $q = f_m(z_m) = f_m(z_{m+1})$ , it follows that  $z_m, z_{m+1} \in \mathbb{C} \setminus \mathbb{R}$ , and by Assumption 2.5 we know  $f'_m(z_m) \neq 0$  as well as  $f'_m(z_{m+1}) \neq 0$ . Then there exist two values  $\alpha_1, \alpha_2 \in (0, \pi)$  such that

$$f_m(r_\varepsilon e^{i\alpha_1(\varepsilon)}) = f_m(r_\varepsilon e^{i\alpha_2(\varepsilon)}) = \tau(\varepsilon). \quad (2.24)$$

Let us also define  $\alpha_0 \in (\alpha_1, \alpha_2)$  such that  $f_m(r_0 e^{i\alpha_0}) = q \in \mathbb{R}$ . Then because of the continuity of  $\alpha(\lambda)$ , in the limit as  $\varepsilon \rightarrow 0$ , it must hold that  $\alpha_1(\varepsilon) \rightarrow \alpha_0$  and  $\alpha_2(\varepsilon) \rightarrow \alpha_0$ . Passing to the limit yields,

$$\lim_{\varepsilon \rightarrow 0} \frac{f_m(r_\varepsilon e^{i\alpha_1(\varepsilon)}) - f_m(r_\varepsilon e^{i\alpha_2(\varepsilon)})}{\alpha_1(\varepsilon) - \alpha_2(\varepsilon)} = \lim_{\varepsilon \rightarrow 0} \frac{0}{\alpha_1(\varepsilon) - \alpha_2(\varepsilon)} = 0. \quad (2.25)$$

Let  $h(\varepsilon) := \alpha_1(\varepsilon) - \alpha_2(\varepsilon)$ , then the limit in (2.25) can be rewritten as,

$$\lim_{\varepsilon \rightarrow 0} \frac{f_m(r_\varepsilon e^{i(\alpha_2(\varepsilon)+h(\varepsilon))}) - f_m(r_\varepsilon e^{i\alpha_2(\varepsilon)})}{h(\varepsilon)} = f'_m(r_0 e^{i\alpha_0}) e^{i\alpha_0}. \quad (2.26)$$

However, by our assumption that  $f'_m(r_0 e^{i\alpha_0}) \neq 0$ , we obtain a contradiction with (2.25), and hence no such path  $\tau$  can exist. In the case  $q = \lambda_1$  or  $q = \lambda_2$  by Assumption 2.5, we have  $z_{m-1} \neq z_m = z_{m+1} \neq z_{m+2}$ . In a similar fashion as in (2.25) the roots at  $\tau(\varepsilon)$  must remain distinct, as otherwise the second derivative would vanish.

The equality in (2.22) is obtained as follows. From (2.14) and the fact that  $\sigma_{\text{open}}(\mathbf{T}(f)) \subseteq \mathbb{R}$ , we deduce that,

$$\sigma_{\text{open}}(\mathbf{T}(f)) = \{\lambda \in \mathbb{R} : |z_m(\lambda)| = |z_{m+1}(\lambda)|\} \quad (2.27)$$

$$= \{f_m(z) : z \in \mathbf{Z}(f_m)\} \quad (2.28)$$

$$= \bigcup_{\alpha \in [-\pi, \pi]} f_m(p(e^{i\alpha})) \quad (2.29)$$

$$= \sigma_{\text{open}}(\mathbf{T}(f_m \circ p)), \quad (2.30)$$

where the last equality follows from the spectral properties of Hermitian Toeplitz matrices [1, Theorem 5.14], and the second to last equality follows from (2.21).  $\square$

For a visualisation of the non-continuity of  $\alpha(\lambda)$ , we refer the reader to Figures 2.2 and A.3. For continuous  $\alpha(\lambda)$  the proof strategy fails when the roots become confluent, which is why we require Assumption 2.5. An illustration of a possible breaking point is provided in Figure A.2.

We proceed to illustrate the case where  $\mathbf{Z}(f_m)$  is spanned by a polar curve in Figure 2.1, in which case the open spectrum is real and, contrarily, an example, where  $\mathbf{Z}(f_m)$  is not spanned by a polar curve in Figure 2.2.

Consequently a visual criterion for when the open limit has real spectrum is if the gap band closest to the origin does not touch or overlap any other gap bands, as the corresponding real band sweeps over the first Brillouin zone. It is worth mentioning that Theorem 2.10 comes as no surprise as it has been conjectured and empirically observed, under weaker assumptions, that is,  $f_m^{-1}(\lambda)$  contains a Jordan curve, which has

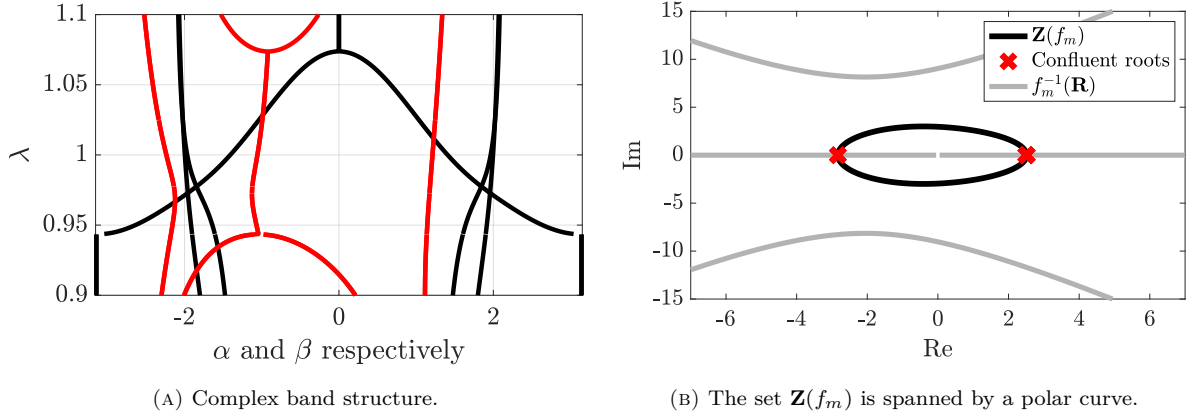


FIGURE 2.1. Clearly the set  $\mathbf{Z}(f_m) \subseteq f_m^{-1}(\mathbb{R})$  is parametrised by a polar curve. We emphasise that confluent roots are only situated on the real axis and by Remark 2.6 belong to  $\mathbf{Z}(f_m)$ . We see that there are no other confluent roots as the complex band in (A) is isolated. Computation performed for  $m = 3$ ,  $\kappa = 3.5$ ,  $\rho = 6.5$ .

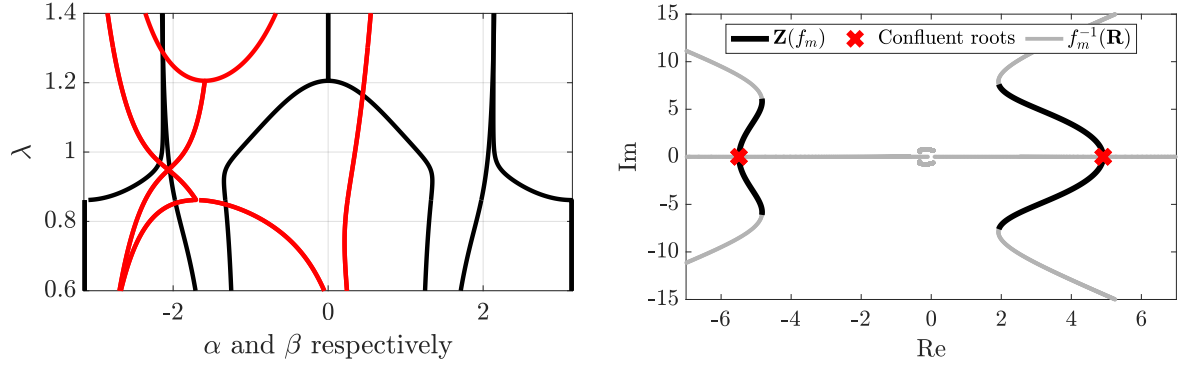


FIGURE 2.2. The set  $\mathbf{Z}(f_m) \subseteq f_m^{-1}(\mathbb{R})$  is no longer parametrised by a polar curve. Equivalently the gap bands in (A) cross each other. The open limit in this setting contains complex values. Computation performed for  $m = 3$ ,  $\kappa = 1$ ,  $\rho = 6.5$ .

been presented in [31, Theorem 1]. However, the proof of this result was later discovered to be erroneous, but despite the error, the result is commonly believed to be true, which is why we state it as a conjecture.

**Conjecture 2.11.** *Let  $f_m$  be the symbol function defined in (2.5), and let us denote by  $f_m^{-1}(\lambda)$  the preimage of the symbol function, i.e. the roots of  $f_m(z) - \lambda = 0$ . The following statements are equivalent,*

- (1) *There exists a Jordan curve parametrised by the complex band structure.*
- (2)  $\lim_{n \rightarrow \infty} \sigma(\mathbf{T}_n(f_m)) \subset \mathbb{R}$ .

Since only the implication (1)  $\Rightarrow$  (2) was affected by the error, the implication (2)  $\Rightarrow$  (1) holds.

**2.2. Asymptotic spectra under homotopic deformations of the unit torus.** As discussed in Theorem 2.10, the open limit is not affected by a specific deformation of the path along which the symbol function is evaluated. In fact, we will see that, the density of states is conserved under such a deformation. The *density of states* (DoS) of a matrix  $\mathbf{A}_n$  is defined as the weak limit as  $n \rightarrow \infty$  of the empirical measures,

$$\mu_n(x) := \frac{1}{n} \sum_{k=1}^n \delta_{\lambda_{k,n}}(x), \quad (2.31)$$

where  $\lambda_{1,n}, \dots, \lambda_{n,n}$  denote the eigenvalues of the matrix  $\mathbf{A}_n$ . For non-Hermitian Toeplitz matrices, the density of states is characterised by the following result [24].

**Theorem 2.12** (Hirschman). *The family of empirical measures  $(\mu_n)_{n \in \mathbb{N}}$  converges weakly to a measure that is supported on  $\sigma_{\text{open}}(\mathbf{T}(f))$  and equals*

$$d\mu = \frac{1}{2\pi} \frac{1}{g} \left| \frac{\partial g}{\partial n_1} + \frac{\partial g}{\partial n_2} \right| ds, \quad (2.32)$$

where  $ds$  is the arc length measure on  $\sigma_{\text{open}}(\mathbf{T}(f))$ . The function  $g$  is defined as,

$$g(\lambda) := |a_m| \prod_{k \in \{m+1, 2m\}} |z_k(\lambda)|, \quad (2.33)$$

and  $z_i(\lambda)$  are the roots of the polynomial equation  $z^m(f_m(z) - \lambda)$  sorted in ascending magnitude,

We now turn to one of the central theorems of this paper, namely that the transformation of the Toeplitz matrix, by evaluating the symbol function on the polar curve  $p(\mathbb{T})$ , can be seen as an asymptotic similarity transform, which on average keeps the eigenvalues the same. This averaging of asymptotic spectra is precisely captured by the density of states.

**Theorem 2.13.** *Suppose that the contour traced out by (2.21) is  $C^1([0, 2\pi])$ , then*

$$\text{DoS}(\mathbf{T}_n(f)) = \text{DoS}(\mathbf{T}_n(f \circ p)). \quad (2.34)$$

*Proof.* Let us start with the matrix  $\mathbf{T}_n(f \circ p)$ , then we know by Theorem 2.10 that

$$\sigma_{\text{open}}(\mathbf{T}_n(f)) = \sigma_{\text{open}}(\mathbf{T}_n(f \circ p)) =: [A, B] \subset \mathbb{R}. \quad (2.35)$$

Let us cover the closed interval  $[A, B]$  with a sequence of open intervals of length  $\varepsilon > 0$ , that is

$$E_i := (a_i, b_i), \quad [A, B] \subset \bigcup_{i \in I} E_i, \quad |a_i - b_i| < \varepsilon. \quad (2.36)$$

Then for each of these Borel subsets  $E_i \subset \mathbb{R}$  it holds by [1, Corollary 5.12.] that the empirical measure converges weakly to the density of states, that is

$$\mu_n(E_i) := \frac{1}{n} \sum_{j=1}^n \chi_{E_i}(\lambda_j(\mathbf{T}_n(f \circ p))) \rightharpoonup \mu(E_i) := \frac{1}{2\pi} \int_0^{2\pi} \chi_{E_i}(f \circ p(e^{i\theta})) d\theta. \quad (2.37)$$

Because the polar curve  $p(e^{i\alpha}) \in C^1([0, 2\pi])$  on the infinitesimal set  $E_i$  it may be locally approximated as being constant. In other words, the density of states becomes,

$$\frac{1}{2\pi} \int_0^{2\pi} \chi_{E_i}(f \circ p(e^{i\theta})) d\theta = \frac{1}{2\pi} \int_0^{2\pi} \chi_{E_i}(f(e^{-\beta(\lambda(\theta))} e^{i\theta})) d\theta \quad (2.38)$$

$$= \frac{1}{2\pi} 2 \int_{\alpha_1}^{\alpha_2} f(e^{-\beta(\theta)} e^{i\alpha}) d\theta \quad (2.39)$$

$$= \frac{1}{\pi} \sum_{k=-m}^m a_k \underbrace{\int_{\alpha_1}^{\alpha_2} r(\theta)^k e^{ik\theta} d\theta}_{=: I_k}. \quad (2.40)$$

In particular on the set  $E_i$ , the integral  $I_k$  can be approximated with a constant radius, that is  $r_0 := r(\theta_0)$ ,  $\theta_0 \in [\alpha_1, \alpha_2]$ , then

$$I_k = r_0^k \int_{\alpha_1}^{\alpha_2} e^{ik\theta} d\theta + Er. \quad (2.41)$$

The error term may be estimated as follows. The function  $x \mapsto x^k$  is Lipschitz continuous on  $[0, 2\pi]$ , and let  $R = \sup_{\theta \in [\alpha_1, \alpha_2]} |r(\theta)|$  then the following estimate holds,

$$|r(\theta)^k - r(\theta_0)^k| \leq kR^{k-1}|r(\theta) - r(\theta_0)| \leq kR^{k-1}L|\theta - \theta_0|. \quad (2.42)$$

Consequently, the error term may be bounded by

$$|Er| = \int_{\alpha_1}^{\alpha_2} |r(\theta)^k - r(\theta_0)^k| d\theta \leq kR^{k-1}L\varepsilon^2 = \mathcal{O}(\varepsilon^2). \quad (2.43)$$

Therefore, for each  $\varepsilon > 0$  we have that,

$$\mu(E_i) = \frac{1}{2\pi} \int_0^{2\pi} \chi_{E_i}(f(r_0 e^{i\theta})) d\theta + \mathcal{O}(\varepsilon^2). \quad (2.44)$$

Let us define the empirical measure for  $\mathbf{T}_n(f)$  as,

$$\nu_n(E_i) := \frac{1}{n} \sum_{j=1}^n \chi_{E_i} \left( \lambda_j \left( \mathbf{T}_n(f(\mathbb{T})) \right) \right) = \frac{1}{n} \sum_{j=1}^n \chi_{E_i} \left( \lambda_j \left( \mathbf{T}_n(f(r\mathbb{T})) \right) \right), \quad (2.45)$$

where in the second equality, we used the fact that the matrices  $\mathbf{T}_n(f(\mathbb{T}))$  and  $\mathbf{T}_n(f(r\mathbb{T}))$  are similar for every  $r > 0$ . In particular, by [1, Corollary 5.12.] and (2.44) it follows that

$$\nu_n(E_i) = \frac{1}{n} \sum_{j=1}^n \chi_{E_i} \left( \lambda_j \left( \mathbf{T}_n(f(r_i\mathbb{T})) \right) \right) \rightharpoonup \mu(E_i) + \mathcal{O}(\varepsilon^2), \quad (2.46)$$

which completes the proof of the theorem.  $\square$

In Figure 2.3 we numerically illustrate the convergence of the empirical measure for a non-Hermitian banded Toeplitz matrix, for which there exists a polar curve along which the symbol function is real-valued.

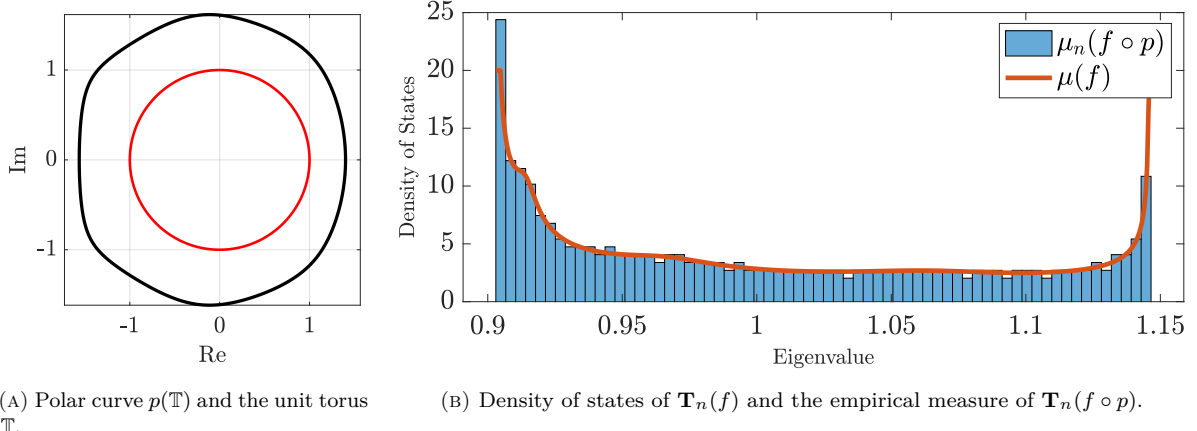


FIGURE 2.3. Figure (A) illustrates the polar curve, which is not just a scaling of the torus but rather a homotopic deformation of the torus. Figure (B) illustrates that even for relatively small matrix sizes, i.e.  $n = 100$ , the empirical measure of  $\mathbf{T}_n(f \circ p)$  approaches the density of states  $\mathbf{T}_n(f)$ . Computation performed for  $\kappa = 3.5$ ,  $\rho = 4.8$  and  $m = 7$ .

In the proof of Theorem 2.13 a formula for the DoS of Hermitian Toeplitz matrices was presented in (2.37). Note that this formula is considerably simpler than the general formula for non-Hermitian Toeplitz matrices presented in (2.32). In other words, to find the density of states for a non-Hermitian matrix  $\mathbf{T}_n(f)$ , it is sufficient to compute the density of states for the Hermitian matrix  $\mathbf{T}_n(f \circ p)$ . We have the following result.

**Corollary 2.14.** *Suppose that the contour traced out by (2.21) is  $C^1([0, 2\pi])$ , then for a Borel subset  $E \subset \mathbb{R}$  the DoS( $\mathbf{T}_n(f)$ ) is given by the measure,*

$$\mu(E) = \frac{1}{2\pi} \int_0^{2\pi} \chi_E(f \circ p(e^{i\theta})) d\theta. \quad (2.47)$$

*Proof.* As the assumptions for Theorem 2.13 are met, computing the DoS of  $\mathbf{T}_n(f)$  is equivalent to computing the DoS of the Hermitian matrix  $\mathbf{T}_n(f \circ p)$ . Following the formula of the density of states of a Hermitian Toeplitz matrix [17, Section 7.5], it follows that the density of states is given by (2.47).  $\square$

In conclusion, the class of non-Hermitian Toeplitz matrices, as intended by Theorem 2.13, many results such as eigenvalues estimates and convergence rates follow from existing results for Hermitian matrices. We refer the reader to [1, 8, 9] for a detailed study of the subject.

**2.3. Density of states of asymptotically equivalent matrices.** In the present section, we demonstrate that the convergence of density of states presented in Theorem 2.13, may also be applied to matrices which are not entry-wise Toeplitz. This result will be of particular importance for considering finite but large physical systems, as the finiteness often incorporates possible edge effects, which may perturb the edge entries of the Toeplitz matrix approximation. We will present results similar to [5] for non-Hermitian matrices with real asymptotic spectra. For an  $n \times n$  matrix  $\mathbf{M}$ , let us define the normalised Frobenius norm as

$$|\mathbf{M}|^2 := \frac{1}{n} \sum_{i,j}^n |\mathbf{M}_{i,j}|. \quad (2.48)$$

**Definition 2.15.** Two sequences of  $n \times n$  matrices  $\mathbf{A}_n$  and  $\mathbf{B}_n$  are said to be *asymptotically equivalent* if they have bounded operator norm, that is,  $\|\mathbf{A}_n\|, \|\mathbf{B}_n\| < \infty$ , and

$$\lim_{r \rightarrow \infty} |\mathbf{A}_r - \mathbf{B}_r| = 0. \quad (2.49)$$

If one of the two matrices is a Toeplitz matrix, then the other is said to be *asymptotically Toeplitz*.

We have the following result for asymptotically equivalent matrices [16, Corollary 2.1].

**Theorem 2.16.** *Let  $\mathbf{A}_n$  and  $\mathbf{B}_n$  be asymptotically equivalent sequences of matrices with eigenvalues  $a_{n,k}$  and  $b_{n,k}$  respectively, then the moments agree, that is,*

$$\lim_{n \rightarrow \infty} \frac{1}{n} \sum_{k=1}^n a_{n,k}^s = \lim_{n \rightarrow \infty} \frac{1}{n} \sum_{k=1}^n b_{n,k}^s, \quad \forall s \in \mathbb{N}. \quad (2.50)$$

Asymptotic equivalence is not sufficient to specify the pointwise behaviour of individual eigenvalues, but it allows one to characterise their density of states. We have the following result on the spectral distribution of asymptotically equivalent matrices.

**Corollary 2.17.** *Let  $\mathbf{A}_n$  be a matrix that is asymptotically equivalent to a Toeplitz matrix  $\mathbf{T}_n$  such that  $\sigma_{\text{open}}(\mathbf{T}_n(f)) \subseteq \mathbb{R}$ , then both matrices asymptotically have the same density of states.*

*Proof.* We have that all moments are finite,

$$\lim_{n \rightarrow \infty} \int x^s d\mu_n^{(\mathbf{A}_n)}(x) = \lim_{n \rightarrow \infty} \frac{1}{n} \sum_{k=1}^n a_{n,k}^s = \lim_{n \rightarrow \infty} \frac{1}{n} \sum_{k=1}^n t_{n,k}^s = \lim_{n \rightarrow \infty} \int x^s d\mu_n^{(\mathbf{T}_n)}(x), \quad \forall s \in \mathbb{N}. \quad (2.51)$$

Moreover, by Theorem 2.12  $\mu_n^{(\mathbf{T}_n)} \rightharpoonup \mu^{(\mathbf{T}_n)}$  and since the measure  $\mu$  is supported on a compact subset of  $\mathbb{R}$ , the moments uniquely determine the measure, from which it follows that  $\mu^{(\mathbf{T}_n)} = \mu^{(\mathbf{A}_n)}$ , which completes the proof.  $\square$

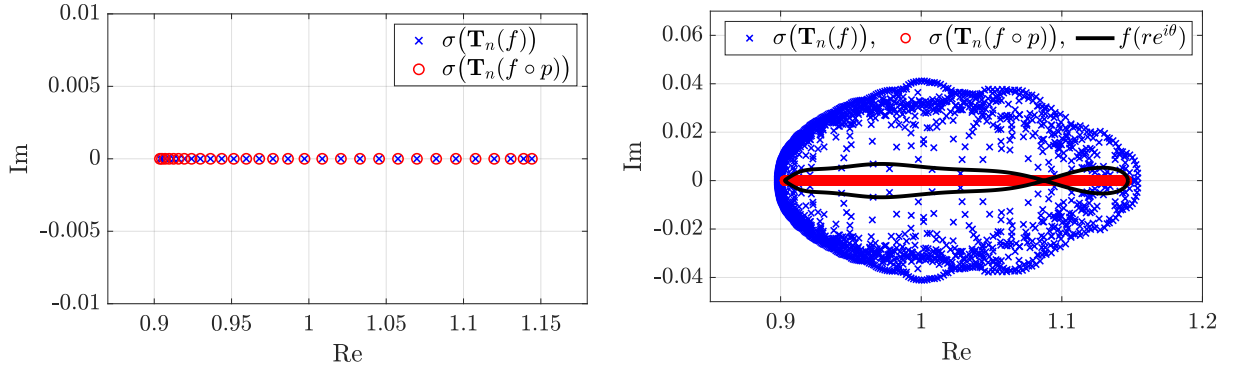
In other words, if a matrix  $\mathbf{A}_n$  is asymptotically equivalent to a Toeplitz matrix  $\mathbf{T}_n$  then their eigenvalues follow the same limiting distribution. This result will be of particular interest when considering the limit of finite but large systems, where the Toeplitz matrix representation may have perturbed entries, due to possible edge effects [2, 10].

**2.4. Asymptotic similarity transform.** A common problem that is often encountered when computing the spectra of large non-Hermitian Toeplitz matrices is numerical pollution, as illustrated in Figure 2.4. This comes from the fact that non-Hermitian Toeplitz matrices are often severely ill-conditioned [8, 29, 34]. This computational bottleneck will be addressed in this section by introducing an asymptotic similarity transform. In order to visualise the spectral pollution, we recall the following result [1, Proposition 2.17.]

**Proposition 2.18.** *If  $f \in L^\infty$ , then  $\sigma(\mathbf{T}_n(f)) \subset \text{conv } \mathcal{R}(f)$ , where  $\mathcal{R}(f)$  is the essential range of  $f$ .*

Consequently, because of the similarity of  $\mathbf{T}_n(f(\mathbb{T})) \sim \mathbf{T}_n(f(r\mathbb{T}))$  choosing  $r$  in such a manner that  $\text{conv } \mathcal{R}(f(r\mathbb{T}))$  has the smallest measure, corresponds to preconditioning the matrix  $\mathbf{T}_n(f(\mathbb{T}))$ , see [7].

In the case of tridiagonal matrices, the problem may be overcome by shrinking  $\text{conv } \mathcal{R}(f(r\mathbb{T}))$  to a line, just by scaling the unit torus with a correctly chosen  $r$ , see [3, 4]. For banded Toeplitz matrices, this collapsing of the unit circle no longer applies as in the tridiagonal case, which is why we will allow general polar curves  $p : \mathbb{T} \rightarrow \mathbb{C}$  instead of just scaling of the unit torus  $p(z) = rz$ . In this manner, we show that under the same assumptions as in Theorem 2.10,  $\text{conv } \mathcal{R}(f \circ p(\mathbb{T}))$  will collapse onto the line.



(a) The numerically computed eigenvalues of  $\mathbf{T}_n(f \circ p)$  and  $\mathbf{T}_n(f)$  for  $n = 40$  agree closely. A more detailed convergence study will be presented in Figure 2.5.

(b) Numerically computed spectra of  $\mathbf{T}_n(f \circ p)$  and  $\mathbf{T}_n(f)$  for  $n = 2000$ . Many of the eigenvalues of  $\mathbf{T}_n(f \circ p)$  fall outside of  $\text{conv} \mathcal{R}(f(r\mathbb{T}))$  and by Proposition 2.18 constitute numerical error.

FIGURE 2.4. The Hermitian matrix  $\mathbf{T}_n(f \circ p)$  is less prone to numerical pollution compared to the non-Hermitian banded Toeplitz matrices, this motivates the idea of considering the evaluation of the symbol function on a deformed torus as a numerical preconditioner. Computation performed for  $\kappa = 3.5$ ,  $\rho = 4.8$  and  $m = 7$ .

For non-Hermitian banded Toeplitz matrices, one may formally consider the asymptotic similarity transform  $\mathbf{T}_n(f) \approx \mathbf{M}^{-1} \mathbf{T}_n(f \circ p) \mathbf{M}$ , where

$$(\mathbf{M})_{i,j} = \frac{1}{2\pi} \int_0^{2\pi} p(e^{i\theta})^j e^{i\theta i} d\theta. \quad (2.52)$$

We would like to emphasise that the asymptotic similarity transform presented in (2.52) is the natural generalisation for the exact similarity transform, given by a scaling of the torus. For a function  $p(z) = rz$  for  $r > 0$ , the transform in (2.52) reduces to the known similarity transform  $\mathbf{M} = \text{diag}(1, r, r^2, \dots, r^n)$ . We emphasise that the similarity transform introduced in (2.52) is exponentially ill-conditioned, which is why we never use it in numerical computations. This is due to the fact that the entries grow or decay exponentially in the index  $j$ . In practical terms, we instead compute the symmetrised matrix  $\mathbf{T}_n(f \circ p)$  by numerically evaluating the Fourier coefficients  $(\widehat{f \circ p})_k$ . More details on the computation of the Fourier coefficients can be found in the Appendix B.

The transform  $\mathbf{T}_n(f) \rightarrow \mathbf{T}_n(f \circ p)$  is expected to not be an exact similarity transform for finite  $n$ . This is due to the fact that the Fourier coefficients  $(\widehat{f \circ p})_k$  are, in general, no longer banded; see, for example, Figure B.1 (B). Consequently, the coefficients  $(\widehat{f \circ p})_k$  for  $|k| > n$  will not influence the matrix  $\mathbf{T}_n(f \circ p)$ . However, we will provide numerical evidence that the spectrum is conserved pointwise under the transform  $\mathbf{T}_n(f) \rightarrow \mathbf{T}_n(f \circ p)$  in Figure 2.5. For more details on the derivation of the similarity transform, we refer the reader to the Appendix C.

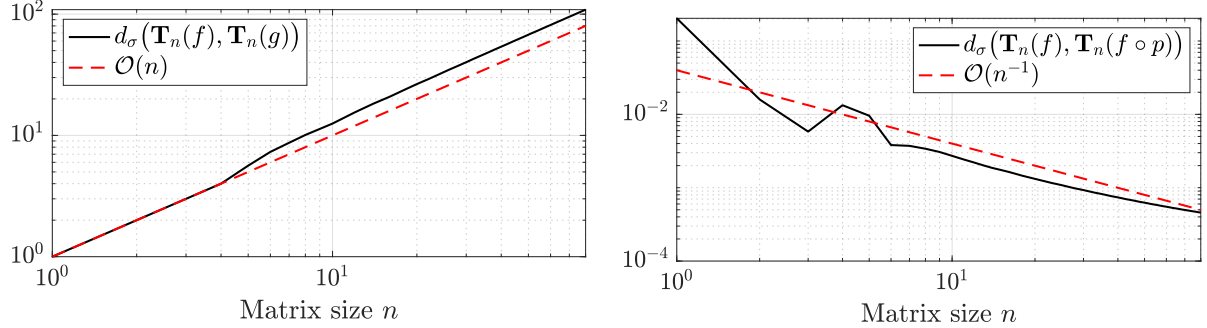
We will consider the error of the spectrum when introducing the transform defined by  $p$ . Let us denote by  $\lambda_k$  and  $\tau_k$  the sorted eigenvalues of  $\mathbf{T}_n(f)$  and  $\mathbf{T}_n(f \circ p)$ , respectively, then we define the  $\ell^1$  distance between the spectra as:

$$d_\sigma(\mathbf{T}_n(f), \mathbf{T}_n(f \circ p)) := \sum_{k=1}^n |\lambda_k - \tau_k|. \quad (2.53)$$

Note that the  $\ell^1$  distance is very sensitive to finitely many outliers, which are enough to ruin the convergence of the  $\ell^1$  distance. Under the assumptions of Theorem 2.10 the eigenvalues of  $\mathbf{T}_n(f)$  and  $\mathbf{T}_n(f \circ p)$  will cluster along the same limiting set which consists of a finite interval on the real axis. As a consequence, it is expected that  $|\lambda_k - \tau_k| = \mathcal{O}(n^{-1})$ . This is the reason why the  $\ell^1$  distance defined in (2.53) does not have a normalisation of  $1/n$ . An illustration of this is given in Remark 2.19.

**Remark 2.19.** We would like to highlight that the observed convergence rate of the spectrum of  $\mathbf{T}_n(f)$  and  $\mathbf{T}_n(f \circ p)$  as  $n$  grows is not simply a consequence of the fact that the limiting spectra agree. For comparison, we consider the symbol functions  $f(\theta) = \cos(\theta)$  and  $g(\theta) = \cos(2\theta)$ , which both correspond

to Hermitian matrices. It is not hard to see that their open spectra agree:  $\sigma_{\text{open}}(f) = \sigma_{\text{open}}(g) = [-1, 1]$  even though their DoS do not agree. The  $\ell^1$  distance of this example is illustrated in Figure 2.5 (A), as it showed that the convergence observed in Figure 2.5 (B) is not a result of progressively filling the open limit with additional eigenvalues.



(A) Computation performed for  $f(\theta) = \cos(\theta)$  and  $g(\theta) = \cos(2\theta)$ . The  $\ell^1$  distance does not converge even though their open limit agree.  
(B) Computation performed for  $m = 7, \kappa = 3.5$  and  $\rho = 4.8$ , i.e. the same Toeplitz matrix as in Figure 2.4 and Figure 2.3.

FIGURE 2.5. Numerical experiments show that the  $\ell^1$  distance behaves like  $\mathcal{O}(n^{-1})$ , for Toeplitz matrices that have a closed polar curve  $p(\mathbb{T})$ . In this computation the sampling size for the FFT scales with the matrix dimension. In this fashion, we achieve a robust numerical framework in which both the numerical errors and the analytical errors scale like  $\mathcal{O}(n^{-1})$ . For more details on this we refer the reader to Appendix B. Note that it is numerically difficult to simulate matrices for sizes larger than  $n = 100$ , see Figure 2.4.

In conclusion, in Theorem 2.13 we demonstrated that the density of states of  $\mathbf{T}_n(f)$  and  $\mathbf{T}_n(f \circ p)$  agrees. However, this is not enough to guarantee pointwise convergence of the asymptotic spectrum, as there might be  $o(n)$  many outliers without affecting the limiting distribution. Despite this, Figure 2.5 provides numerical corroboration that the transform  $\mathbf{T}_n(f) \rightarrow \mathbf{T}_n(f \circ p)$  can be seen as an asymptotic similarity transform.

### 3. NON-HERMITIAN BLOCH HAMILTONIANS: OPEN AND PERIODIC BOUNDARY CONDITIONS

Toeplitz matrix models find applications especially in the theory of condensed matter, for example, in tight-binding electron models and open crystal structures [26, 32]. In the limit as the matrix size tends to infinity, the energy spectrum becomes a piecewise continuous function, which we shall refer to as the open limit. Non-Hermitian Hamiltonians are generally sensitive to boundary conditions, and the asymptotic spectra under open boundary conditions generally do not agree with the Bloch spectrum predicted for periodic boundary conditions [18, 23, 37, 38]. However, using the insights gained in Section 2, in particular Theorem 2.10 will be used to provide a mathematical foundation for the generalised Brillouin zone, capable of capturing the open spectra of non-Hermitian Hamiltonians [40]. In the generalised Brillouin zone, the Bloch wave number is complex valued [15]. In systems involving Bloch Hamiltonians, the complex valued Bloch parameter is often called an *imaginary gauge transformation*, relating non-reciprocal systems to equivalent Hermitian systems via a similarity transformation. Moreover, Theorem 2.10 gives a visually striking condition: if the generalised Brillouin zone winds once around the origin and is  $C^1$ , then the energy spectrum under open boundary conditions will be real.

For non-Hermitian Hamiltonians, two limits are considered. Periodic boundary conditions (PBC), semi-infinite boundary conditions (SIBC) and open boundary conditions (OBC). In [21, 27] an imaginary gauge transformation on the Bloch Hamiltonian is considered,

$$H(e^{i\alpha}) \mapsto H(e^{i(\alpha+ir)}) =: H_r. \quad (3.1)$$

Note that the imaginary gauge potential  $r$  is independent of the Bloch parameter  $\alpha$  and will therefore be denoted as *constant gauge transform*. This transformation does not alter the OBC spectra because it is implemented as a similarity transformation at the matrix level. By Theorem 2.2, the spectrum of the open

limit of a non-Hermitian resonator chain is given by the intersection of the spectra of the Hamiltonian under all constant imaginary gauge transformations [28], that is

$$\sigma_{\text{OBC}}(H) = \bigcap_{r \in (0, \infty)} \sigma_{\text{SIBC}}(H_r). \quad (3.2)$$

The downside of this characterisation is that it is in general hard to conceptualise infinite intersections. We may evade taking infinite intersections in (3.2) provided that the assumptions of Theorem 2.10 are met. In this case, the open limit is captured by evaluating the Bloch Hamiltonian along the curve specified by  $p : \mathbb{T} \rightarrow \mathbb{C}$ , such that

$$\sigma_{\text{OBC}}(H) = \bigcup_{\alpha \in [-\pi, \pi]} \sigma(H(p(e^{i\alpha}))). \quad (3.3)$$

The key assumption of Theorem 2.10 is that the generalised Brillouin zone is spanned by a polar curve  $p(\mathbb{T})$ . This assumption naturally appears in (3.3): the imaginary gauge transform  $e^{i\alpha} \rightarrow p(e^{i\alpha})$  is uniquely specified by the Bloch parameter  $\alpha$ .

Depending on the relative position of the generalised Brillouin zone with respect to the unit torus, we may observe left or right eigenmode condensation. When the generalised Brillouin zone crosses the unit circle, bulk eigenmodes become partially left-localised and partially right-localised [22, 25]. This is numerically illustrated in Figure 3.1

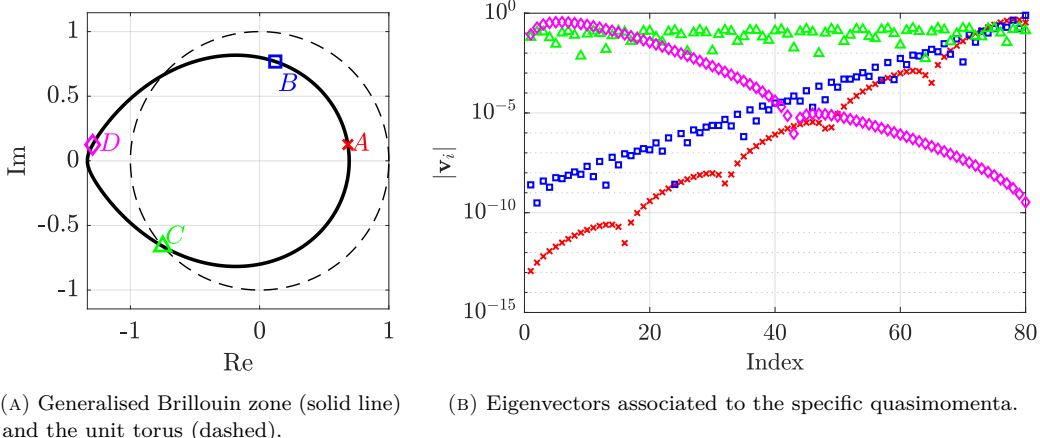


FIGURE 3.1. Generalised Brillouin zone for a long-range non-Hermitian Hamiltonian  $H(z) = 0.6z^{-2} + 2.5z^{-1} + 3.2 + 1.6z$ . As the Brillouin zone is traced out by a polar curve, by Theorem 2.10, the open spectrum will be real. The decay rate of the eigenmodes associated to certain quasimomenta is correctly predicted by the generalised Brillouin zone.

#### 4. CONCLUDING REMARKS

In this work, we analysed the asymptotic spectra of banded non-Hermitian Toeplitz matrices and established a rigorous mathematical foundation for the generalised Brillouin zone in non-Hermitian systems. In future work, we plan to illustrate these results in a concrete PDE setting, showing that for periodic systems of non-Hermitian partial differential equations, the complex quasimomentum must also depend on the Floquet parameter. It would also be interesting to explore applications to specific models, such as the long-range Hatano–Nelson model or the subwavelength non-Hermitian skin effect.

#### 5. DATA AVAILABILITY

The **Matlab** code for the numerical experiments developed in this work is openly available in the following repository: <https://github.com/yannick2305/OpenLimitToeplitz>.

## REFERENCES

- [1] Böttcher Albrecht and Silbermann Bernd. *Introduction to Large Truncated Toeplitz Matrices*. Springer New York, NY, 1998. doi: 10.1007/978-1-4612-1426-7.
- [2] Habib Ammari, Silvio Barandun, Jinghao Cao, Bryn Davies, Erik Orvehed Hiltunen and Ping Liu. ‘The Non-Hermitian Skin Effect With Three-Dimensional Long-Range Coupling’. In: *Journal of the European Mathematical Society (published online first)* Vol (2025).
- [3] Habib Ammari, Silvio Barandun, Yannick De Bruijn, Ping Liu and Clemens Thalhammer. ‘Spectra and pseudo-spectra of tridiagonal  $k$ -Toeplitz matrices and the topological origin of the non-Hermitian skin effect’. In: *Journal of Physics A: Mathematical and Theoretical* 58 Vol 20 (2025), p. 205201. doi: 10.1088/1751-8121/add5ab.
- [4] Habib Ammari, Silvio Barandun, Ping Liu and Alexander Uhlmann. ‘Generalised Brillouin Zone for Non-Reciprocal Systems’. In: *Proc. R. Soc. A* 481 Vol (2025), p. 20240643. doi: 10.1098/rspa.2024.0643.
- [5] Habib Ammari, Bryn Davies and Erik Orvehed Hiltunen. ‘Spectral convergence in large finite resonator arrays: The essential spectrum and band structure’. In: *Bulletin of the London Mathematical Society* 57 Vol 3 (2025), pp. 730–747. doi: <https://doi.org/10.1112/blms.13225>.
- [6] Yuto Ashida, Zongping Gong and Masahito Ueda. ‘Non-Hermitian Physics’. In: *Advances in Physics* 69 Vol 3 (2020), pp. 249–435. doi: 10.1080/00018732.2021.1876991.
- [7] Richard M. Beam and Robert F. Warming. ‘The Asymptotic Spectra of Banded Toeplitz and Quasi-Toeplitz Matrices’. In: *SIAM J. Sci. Comput.* 14 Vol (1993), pp. 971–1006. doi: 10.1137/0914059.
- [8] M. Bogoya and S. M. Grudsky. ‘Eigenvalues of Non-Hermitian Banded Toeplitz Matrices Approaching Simple Points of the Limiting Set’. In: *Computational Mathematics and Mathematical Physics* 65 Vol 7 (2025), pp. 1453–1471. doi: 10.1134/S0965542525700745.
- [9] Albrecht Böttcher and Sergei M. Grudsky. *Spectral Properties of Banded Toeplitz Matrices*. Society for Industrial and Applied Mathematics, 2005. doi: 10.1137/1.9780898717853.
- [10] Yannick de Bruijn, Bryn Davies, Sacha Dupuy and Erik Orvehed Hiltunen. *Spectra and pseudospectra of non-Hermitian Toeplitz operators: Eigenvector decay transitions in banded and dense matrices*. 2025. arXiv: 2512.03757 [math.AP].
- [11] Yannick De Bruijn and Erik Orvehed Hiltunen. *Complex Band Structure and localisation transition for tridiagonal non-Hermitian  $k$ -Toeplitz operators with defects*. 2025. arXiv: 2505.23610 [math.AP].
- [12] Yannick De Bruijn and Erik Orvehed Hiltunen. *Complex Brillouin Zone for Localised Modes in Hermitian and Non-Hermitian Problems*. 2025. arXiv: 2502.06620 [math.AP].
- [13] Teodor Bucht and Jacob S. Christiansen. ‘A Geometric Approach to Approximating the Limit Set of Eigenvalues for Banded Toeplitz Matrices’. In: *SIAM Journal on Matrix Analysis and Applications* 45 Vol 3 (2024), pp. 1573–1598. doi: 10.1137/23M1587804.
- [14] B. Davies, S. Barandun, E. O. Hiltunen, R. V. Craster and H. Ammari. ‘Two-scale effective model for defect-induced localization transitions in non-Hermitian systems’. In: *Phys. Rev. B* 111 Vol (2025), p. 035109. doi: 10.1103/PhysRevB.111.035109.
- [15] Yannick De Bruijn and Erik Orvehed Hiltunen. ‘Complex Band Structure for Subwavelength Evanescent Waves’. In: *Studies in Applied Mathematics* 154 Vol 2 (2025), e70022. doi: 10.1111/sapm.70022.
- [16] R. Gray. ‘On the asymptotic eigenvalue distribution of Toeplitz matrices’. In: *IEEE Transactions on Information Theory* 18 Vol 6 (1972), pp. 725–730. doi: 10.1109/TIT.1972.1054924.
- [17] Ulf Grenander and Gabor Szego. *Toeplitz Forms and Their Applications*. Berkeley: University of California Press, 1958. ISBN: 9780520355408. doi: 10.1525/9780520355408.
- [18] Gang-Feng Guo, Xi-Xi Bao and Lei Tan. *The Analysis of Bulk Boundary Correspondence under the Singularity of the Generalized Brillouin Zone in Non-Hermitian System*. 2021. arXiv: 2106.06384 [cond-mat.mes-hall].
- [19] Naomichi Hatano and David R. Nelson. ‘Localization Transitions in Non-Hermitian Quantum Mechanics’. In: *Phys. Rev. Lett.* 77 Vol 3 (1996), pp. 570–573. doi: 10.1103/PhysRevLett.77.570.
- [20] Naomichi Hatano and David R. Nelson. ‘Non-Hermitian delocalization and eigenfunctions’. In: *Phys. Rev. B* 58 Vol 13 (1998), pp. 8384–8390. doi: 10.1103/PhysRevB.58.8384.
- [21] Haiping Hu. ‘Topological origin of non-Hermitian skin effect in higher dimensions and uniform spectra’. In: *Science Bulletin* 70 Vol 1 (2025), pp. 51–57. ISSN: 2095-9273. doi: 10.1016/j.scib.2024.07.022.

- [22] Yu-Min Hu, Yin-Quan Huang, Wen-Tan Xue and Zhong Wang. ‘Non-Bloch band theory for non-Hermitian continuum systems’. In: *Phys. Rev. B* 110 Vol 20 (2024), p. 205429. DOI: 10.1103/PhysRevB.110.205429.
- [23] Xiang Ji and Xiaosen Yang. ‘Generalized bulk-boundary correspondence in periodically driven non-Hermitian systems’. In: *Journal of Physics: Condensed Matter* 36 Vol 24 (2024), p. 243001. DOI: 10.1088/1361-648X/ad2c73.
- [24] I. I. Hirschman Jr. ‘The spectra of certain Toeplitz matrices’. In: *Illinois Journal of Mathematics* 11 Vol 1 (1967), pp. 145–159. DOI: 10.1215/ijm/1256054792.
- [25] Wei Li, Zhoujian Sun, Ze Yang and Fuxiang Li. ‘Universal scalefree non-Hermitian skin effect near the Bloch point’. In: *Phys. Rev. B* 109 Vol 3 (2024), p. 035119. DOI: 10.1103/PhysRevB.109.035119.
- [26] A M Marques and R G Dias. ‘Analytical solution of open crystalline linear 1D tight-binding models’. In: *Journal of Physics A: Mathematical and Theoretical* 53 Vol 7 (2020), p. 075303. DOI: 10.1088/1751-8121/ab6a6e.
- [27] Nobuyuki Okuma, Kohei Kawabata, Ken Shiozaki and Masatoshi Sato. ‘Topological Origin of Non-Hermitian Skin Effects’. In: *Physical Review Letters* 124 Vol 8 (2020). DOI: 10.1103/PhysRevLett.124.086801.
- [28] Nobuyuki Okuma and Masatoshi Sato. ‘Non-Hermitian Topological Phenomena: A Review’. In: *Annual Review of Condensed Matter Physics* 14 Vol Volume 14, 2023 (2023), pp. 83–107. ISSN: 1947-5462. DOI: 10.1146/annurev-conmatphys-040521-033133.
- [29] Lothar Reichel and Lloyd N. Trefethen. ‘Eigenvalues and pseudo-eigenvalues of Toeplitz matrices’. In: *Linear Algebra and its Applications* 162–164 Vol (1992), pp. 153–185. ISSN: 0024-3795. DOI: 10.1016/0024-3795(92)90374-J.
- [30] Palle Schmidt and Frank Spitzer. ‘The Toeplitz Matrices of an Arbitrary Laurent Polynomial.’ In: *Mathematica Scandinavica* 8 Vol (15–38 1960), pp. 15–38. DOI: 10.7146/math.scand.a-10588.
- [31] Boris Shapiro and Frantisek Stampach. ‘Non-Self-Adjoint Toeplitz Matrices Whose Principal Submatrices Have Real Spectrum’. In: *Constructive Approximation* 49 Vol 2 (2019), pp. 191–226. DOI: 10.1007/s00365-017-9408-0.
- [32] G.C. Stey. ‘Quantum dynamics in Toeplitz hamiltonian systems’. In: *Physica* 68 Vol 2 (1973), pp. 213–242. ISSN: 0031-8914. DOI: 10.1016/0031-8914(73)90098-0.
- [33] Otto Toeplitz. ‘Zur Theorie der quadratischen und bilinearen Formen von unendlichvielen Veränderlichen’. In: *Mathematische Annalen* 70 Vol 3 (1911), pp. 351–376. DOI: 10.1007/BF01564502.
- [34] Lloyd N. Trefethen and Mark Embree. *Spectra and Pseudospectra*. Princeton University Press, Princeton, NJ, 2005. DOI: 10.1515/9780691213101.
- [35] J. L. Ullman. ‘A problem of Schmidt and Spitzer’. In: *Bulletin of the American Mathematical Society* 73 Vol 6 (1967), pp. 883–885. DOI: 10.1090/s0002-9904-1967-11826-3.
- [36] Harold Widom. ‘On the spectrum of a Toeplitz Operator’. In: *Pacific Journal of Mathematics* Vol. 14 Vol 1 (1964), pp. 365–375. DOI: 10.2140/pjm.1964.14.365.
- [37] Deguang Wu, Jiao Xie, Yao Zhou and Jin An. ‘Connections between the open-boundary spectrum and the generalized Brillouin zone in non-Hermitian systems’. In: *Phys. Rev. B* 105 Vol 4 (2022), p. 045422. DOI: 10.1103/PhysRevB.105.045422.
- [38] Zhesen Yang, Kai Zhang, Chen Fang and Jiangping Hu. ‘Non-Hermitian Bulk-Boundary Correspondence and Auxiliary Generalized Brillouin Zone Theory’. In: *Physical Review Letters* 125 Vol 22 (2020). ISSN: 1079-7114. DOI: 10.1103/physrevlett.125.226402.
- [39] Shunyu Yao and Zhong Wang. ‘Edge States and Topological Invariants of Non-Hermitian Systems’. In: *Phys. Rev. Lett.* 121 Vol 8 (2018), p. 086803. DOI: 10.1103/PhysRevLett.121.086803.
- [40] Kazuki Yokomizo and Shuichi Murakami. ‘Non-Bloch Band Theory of Non-Hermitian Systems’. In: *Phys. Rev. Lett.* 123 Vol 6 (2019), p. 066404. DOI: 10.1103/PhysRevLett.123.066404.
- [41] Kai Zhang, Zhesen Yang and Chen Fang. ‘Correspondence between Winding Numbers and Skin Modes in Non-Hermitian Systems’. In: *Phys. Rev. Lett.* 125 Vol 12 (2020), p. 126402. DOI: 10.1103/PhysRevLett.125.126402.

#### APPENDIX A. CONFLUENT ROOTS: OBSTRUCTION IN THE PROOF STRATEGY

In this section, we examine where the proof strategy for Theorem 2.10 may fail when the assumptions of distinct roots is not satisfied. In this setting the technique in the proof fails as the path  $\tau$  to the real axis might be chosen in such a way that the roots become confluent on the real axis. This could lead to

a possible bifurcation into the complex plane. Though we have not yet observed this for some symbol function, as effectively the parameters are poised on a set of measure zero, we will present a possible obstruction in Figure A.2. We recall that following Conjecture 2.11 the result is commonly believed to hold even in the general case, but as of today we can not prove the most general setting yet.

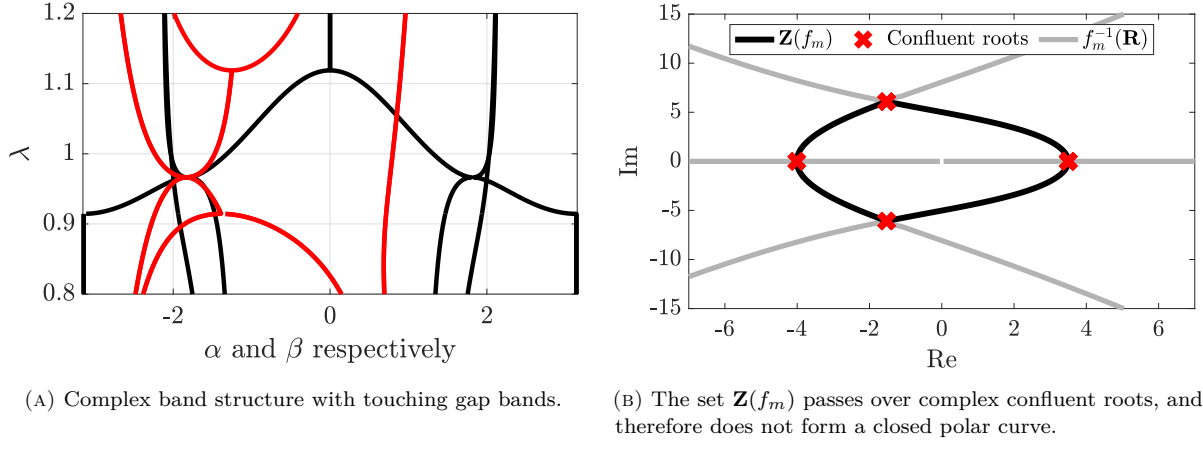


FIGURE A.1. The set  $Z(f_m) \subseteq f_m^{-1}(\mathbb{R})$  is no longer parametrised by a polar curve, as by Remark 2.6, the complex confluent root is not in  $Z(f_m)$ . Therefore  $Z(f_m)$  consists of two disjoint algebraic curves and are thus not spanned by a polar curve. The touching of the complex bands in (A) indicates the presence of confluent complex roots.. Computation performed for  $m = 3$ ,  $\kappa = 2.3052155325$ ,  $\rho = 6.5$ .

If confluent roots were permitted, one could, at least in theory, obtain a situation like the one shown in Figure A.2. We stress that the symbol function and the open spectrum shown are schematic illustrations rather than plots of a specific symbol function. Their purpose is solely to demonstrate potential issues in the confluent case, where a bifurcation in the complex plane may occur.

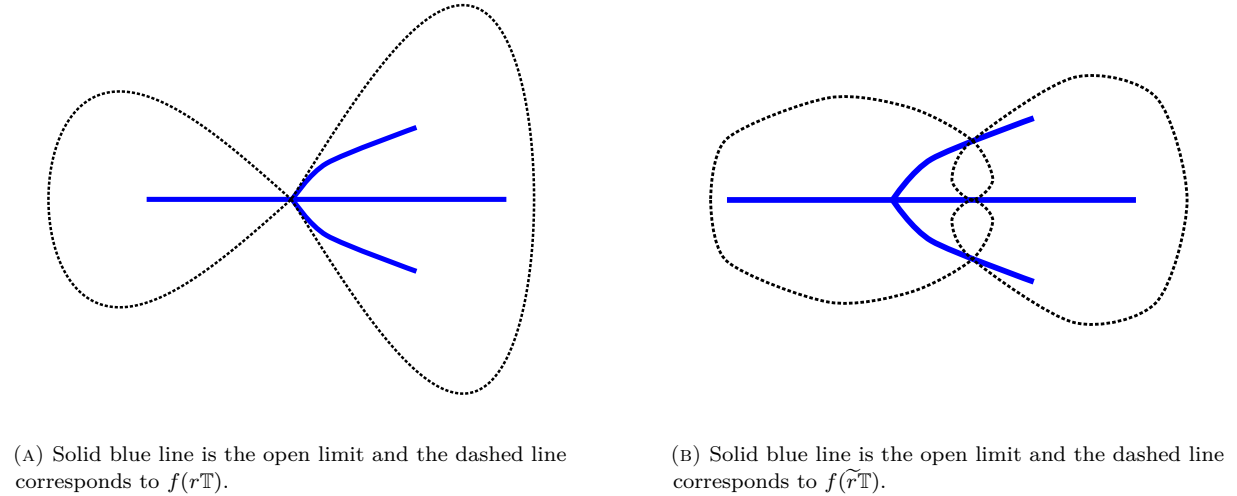
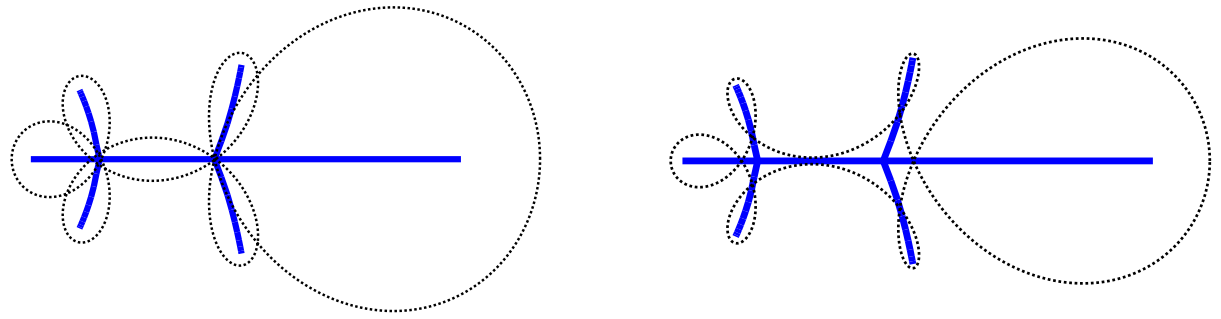


FIGURE A.2. A schematic counterexample illustrating a potential failure point for complex-valued confluent roots, specifically showing how the key argument in the proof of Theorem 2.10 can break down even when  $\alpha(\lambda)$  is continuous. Possibly, this could lead to a bifurcation of  $\sigma_{\text{open}}$  into the complex plane.

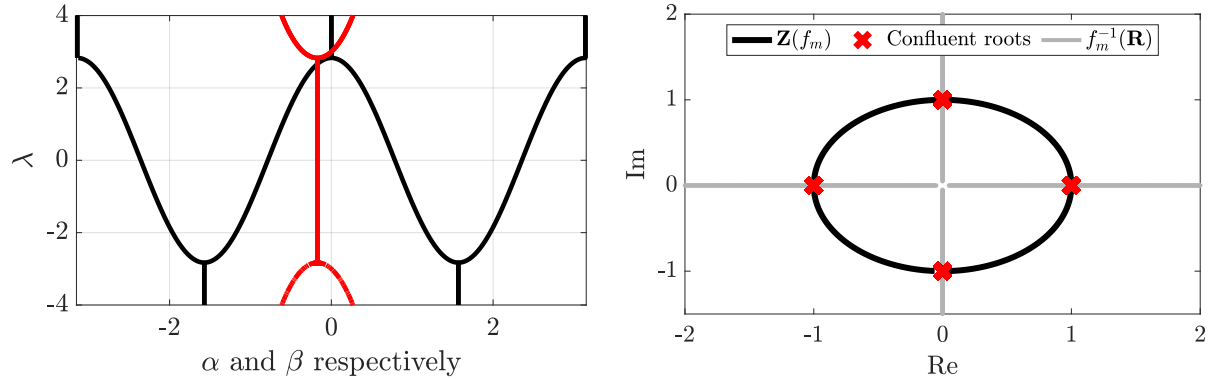
The next result numerically illustrates that the assumptions in Theorem 2.10 are too strong. Namely, the assumption of Conjecture 2.11 that  $f_m^{-1}(\mathbb{R})$  contains a Jordan curve seems to be optimal, this is illustrated in Figure A.4.



(A) Solid blue line is the open limit and the dashed line corresponds to  $f(r\mathbb{T})$  for  $r = 4.97$ .

(B) Solid blue line is the open limit and the dashed line corresponds to  $f(r\mathbb{T})$  for  $r = 4.7$ .

FIGURE A.3. From visual inspection, it is immediately apparent that  $\alpha(\lambda)$  is not continuous at the point where the open limit branches into the complex plane. However, if the set  $\mathbf{Z}(f_m)$  is parametrized by a polar curve according to (2.21), then  $\alpha(\lambda)$  is known to be continuous, which rules out the appearance of such branching behaviour as shown in this figure. Computation performed for  $m = 3$ ,  $\kappa = 1$  and  $\rho = 6$ .



(A) Complex band structure with non-monotone  $\alpha(\lambda)$  band.

(B) The complex valued confluent roots are not part of the set  $\mathbf{Z}(f_m)$ .

FIGURE A.4. The complex-valued confluent points do not belong to the set  $\mathbf{Z}(f_m)$  introduced in (2.17). As a consequence,  $\mathbf{Z}(f_m)$  is not generated by a polar curve, and Theorem 2.10 does not apply. Nonetheless, the open spectrum remains real. Computation performed for a symbol function  $f_m(z) = z^{-2} + 2z^2$ .

## APPENDIX B. NUMERICAL ANALYSIS

In this section, we present the numerical procedure employed to compute the Fourier coefficients  $(\widehat{f \circ p})_k$ . For a given range, we compute the roots of  $z^m(f_m(z) - \lambda)$  sorted by ascending magnitude and keep the roots if  $|z_m(\lambda)| = |z_{m+1}(\lambda)|$ . The set of roots that satisfy this condition constitutes a discrete sampling of a continuous curve  $p(e^{i\theta})$ , where the sampling of the curve is given by non-uniform angles  $\theta_k$  for  $1 \leq k \leq N$ . Then the Fourier coefficients are evaluated by means of the Fast Fourier transform (FFT) with non-uniform sampling. By the Nyquist–Shannon sampling theorem for the Fast Fourier transform, the sample size  $N$  must be at least twice the bandwidth of the signal to avoid aliasing. Because the sample size remains fixed (and does not scale with the size of the matrix), entries outside a certain bandwidth will eventually be polluted due to aliasing. This is the reason we discard the high-frequency coefficients of  $(\widehat{f \circ p})_k$ . This can be formally established by the following result,

**Corollary B.1.** *Consider the Hermitian Toeplitz matrix  $\mathbf{T}_n(f \circ p)$  as well as the  $t$ -banded approximation  $\mathbf{T}_n((f \circ p)_t)$ , and let  $\lambda_k$  and  $\tau_k$ , for  $1 \leq k \leq n$  be the sorted eigenvalues, then it holds that*

$$|\lambda_k - \tau_k| \leq \mathcal{O}((\widehat{f \circ p})_t). \quad (\text{B.1})$$

*Proof.* Let us start by writing

$$\mathbf{T}_n((f \circ p)_t) + \mathbf{E}_t = \mathbf{T}_n(f \circ p), \quad (\text{B.2})$$

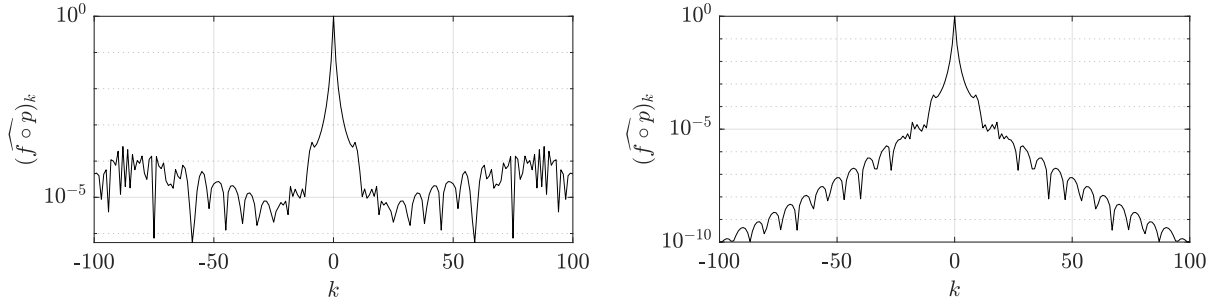
where  $\mathbf{E}_t$  is a Toeplitz matrix comprising the coefficients  $(\widehat{f \circ p})_k$ ,  $t \leq |k| \leq n$ . As the Fourier coefficients  $(\widehat{f \circ p})_{|k|}$  are decaying in  $k$  we may estimate the norm,

$$\|\mathbf{E}_t\|_2 = \mathcal{O}((\widehat{f \circ p})_t). \quad (\text{B.3})$$

By Weyl's theorem on the spectral stability, it follows that

$$|\lambda_k - \tau_k| \leq \mathcal{O}((\widehat{f \circ p})_t), \quad 1 \leq k \leq n, \quad (\text{B.4})$$

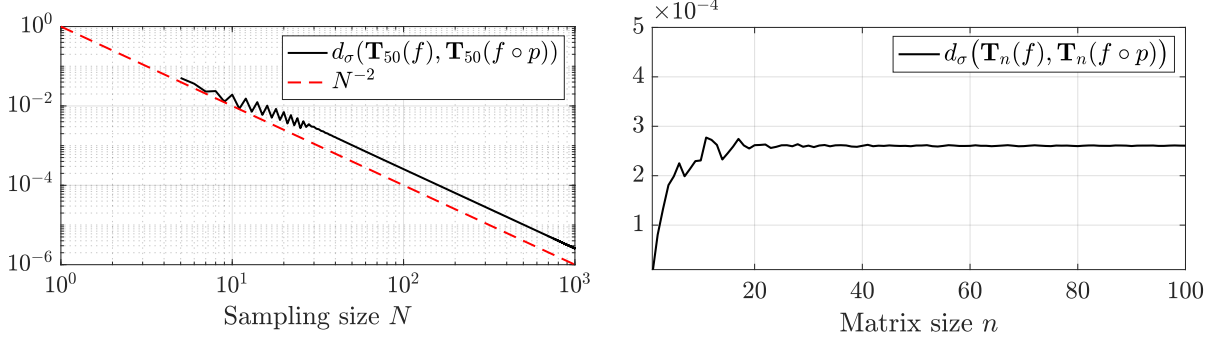
which completes the proof.  $\square$



(a) Fourier coefficients computed for 100 sampling points in the FFT.  
(b) Fourier coefficients computed for 1000 sampling points in the FFT.

FIGURE B.1. Once the bandwidth exceeds a certain threshold, the numerically evaluated Fourier coefficients begin to oscillate instead of decaying, which motivates the need for Corollary B.1.

For analytical functions, the FFT is known to be exponentially convergent. However, for functions that are  $C^k$ , the numerical error is expected to be  $\mathcal{O}(N^{-k})$ . We analyse the numerical error relating to the FFT together with the pointwise spectral convergence, illustrated in Figure B.2. As it turns out, the spectral convergence is very fast, see Figure B.2, and therefore the dominant error will always result from the FFT with respect to the sampling size.



(a) Convergence of the  $\ell^1$  distance under increasing number of sampling points.  
(b) The  $\ell^1$  distance of the spectrum, computed for an FFT sampling of 1000 points.

FIGURE B.2. Numerical experiments indicate that the  $\ell^1$  distance remains independent of the matrix dimension, which in turn yields  $|\lambda_k - \tau_k| = \mathcal{O}(N^{-1})$ , where  $N$  denotes the matrix size. Moreover, the  $\ell^1$  distance can be made small by increasing the number of sampling points in the FFT, highlighting that any observed spectral pollution is in fact due to errors in the discrete Fourier transform.

### APPENDIX C. DERIVATION OF THE SIMILARITY TRANSFORM

In this section, we will formally derive a similarity transform presented in Section 2.4 between  $\mathbf{T}_n(f)$  and  $\mathbf{T}_n(f \circ p)$  for general polar curves  $p : \mathbb{T} \rightarrow \mathbb{C}$ . For the doubly infinite Toeplitz matrix  $\mathbf{T}_n(f)$  in the limit as  $n \rightarrow \infty$  it holds

$$\mathbf{T}_n(f) \approx \mathbf{M}^{-1} \mathbf{T}_n(f \circ p) \mathbf{M}, \quad (\text{C.1})$$

implying that the matrices are asymptotically similar, where the entries of  $\mathbf{M}$  are given by

$$(\mathbf{M})_{i,j} = \frac{1}{2\pi} \int_0^{2\pi} p(e^{i\theta})^j e^{-i\theta i} d\theta, \quad \text{for } i, j \in \mathbb{Z}, \quad (\text{C.2})$$

and correspond to the  $i$ -th Fourier coefficient of  $p : \mathbb{T} \rightarrow \mathbb{C}$  raised to the  $j$ -th power. To see this, consider the  $m$ -banded Toeplitz matrix  $\mathbf{T}_n(f)$  that is generated by the sequence  $\{a_n\}_{n \in \mathbb{Z}}$  such that

$$f(e^{i\theta}) = \sum_{k=-m}^m a_k e^{-i\theta k}, \quad \text{and} \quad f(p(e^{i\theta})) = \sum_{k=-m}^m a_k p(e^{i\theta})^{-k}. \quad (\text{C.3})$$

Let us start by noting that the transformed Toeplitz matrix  $\mathbf{T}_n(f \circ p)$  is generated by the sequence

$$(\widehat{f \circ p})_j = \frac{1}{2\pi} \int_0^{2\pi} f(p(e^{i\theta})) e^{-ij\theta} d\theta = \frac{1}{2\pi} \int_0^{2\pi} \sum_{k=-m}^m a_k p(e^{i\theta})^k e^{-ij\theta} d\theta = \frac{1}{2\pi} \sum_{k=-m}^m a_k \int_0^{2\pi} p(e^{i\theta})^k e^{-i\theta j} d\theta. \quad (\text{C.4})$$

As a result, it follows that,

$$c_n = \frac{1}{2\pi} \sum_{k=-m}^m (\mathbf{M})_{n,k} a_k, \quad \text{and} \quad f(p(e^{i\theta})) = \sum_{k \in \mathbb{Z}} c_k e^{-i\theta k}. \quad (\text{C.5})$$

We have that

$$(\mathbf{M}\mathbf{T}(f))_{i,j} = \sum_{k \in \mathbb{Z}} (\mathbf{M})_{i,k} (\mathbf{T}(f))_{k,j} = \sum_{k \in \mathbb{Z}} (\mathbf{M})_{i,k} a_{k-j} = \sum_{k'=-m}^m (\mathbf{M})_{i,k'+j} a_{k'}, \quad (\text{C.6})$$

as well as

$$(\mathbf{T}(f \circ p)\mathbf{M})_{i,j} = \sum_{k \in \mathbb{Z}} (\mathbf{T}(f \circ p))_{i,k} (\mathbf{M})_{k,j} = \sum_{k'=-m}^m \left( \sum_{k \in \mathbb{Z}} (\mathbf{M})_{i-k,k'} (\mathbf{M})_{k,j} \right) a_{k'}. \quad (\text{C.7})$$

The only thing left to verify is that we have equality between (C.6) and (C.7), so it is enough to verify

$$\sum_{k \in \mathbb{Z}} (\mathbf{M})_{i-k,k'} (\mathbf{M})_{k,j} = (\mathbf{M})_{i,k'+j}. \quad (\text{C.8})$$

Suppose that the function  $p : \mathbb{T} \rightarrow \mathbb{C}$  admits the following Fourier expansion

$$p(e^{i\theta}) = \sum_{n \in \mathbb{Z}} b_n e^{-in\theta}, \quad b_n := \frac{1}{2\pi} \int_0^{2\pi} p(e^{i\theta}) e^{-in\theta} d\theta. \quad (\text{C.9})$$

Then it holds that

$$p(e^{i\theta})^j = \left( \sum_{k \in \mathbb{Z}} b_k e^{-ik\theta} \right)^j = \sum_{i \in \mathbb{Z}} (\mathbf{M})_{i,j} e^{-ii\theta} \quad (\text{C.10})$$

and from the convolution theorem it is clear that  $(\mathbf{M})_{i,j} = (b^{*j})_i$ . We find the convolution type identity,

$$\sum_{k \in \mathbb{Z}} (\mathbf{M})_{i-k,k'} (\mathbf{M})_{k,j} = \sum_{k \in \mathbb{Z}} (b^{*k'})_{i-k} (b^{*j})_k = (b^{*k'} * b^{*j})_i = (b^{*(k'+j)})_i = (\mathbf{M})_{i,k'+j}. \quad (\text{C.11})$$

We stress that asymptotic similarity alone is still insufficient to ensure pointwise convergence of the eigenvalues. Indeed, writing  $\mathbf{T}_n(f) = \mathbf{M}^{-1} \mathbf{T}_n(f \circ p) \mathbf{M} + \mathbf{E}_n$  with  $\|\mathbf{E}_n\| \xrightarrow{n \rightarrow \infty} 0$ , we know from Corollary 2.17 that their densities of states coincide. However, this does not generally yield pointwise control of the eigenvalues.

YANNICK DE BRUIJN

DEPARTMENT OF MATHEMATICS, UNIVERSITY OF OSLO, MOLTKE MOES VEI 35, 0851 OSLO, NORWAY.

ORCID.ORG/0009-0009-6194-0761

Email address: [yannicd@math.uio.no](mailto:yannicd@math.uio.no)

ERIK ORVEHED HILTUNEN

DEPARTMENT OF MATHEMATICS, UNIVERSITY OF OSLO, MOLTKE MOES VEI 35, 0851 OSLO, NORWAY.

ORCID.ORG/0000-0003-2891-9396

Email address: [erikhilt@math.uio.no](mailto:erikhilt@math.uio.no)